Target-density effects in muonic-atom cascades

J. D. Knight, C. J. Orth, and M. E. Schillaci
Los Alamos National Laboratory, Los Alamos, New Mexico 87545

R. A. Naumann
Princeton University, Princeton, New Jersey 08540

F. J. Hartmann
Los Alamos National Laboratory, Los Alamos, New Mexico 87545
and Technical University of Munich, D-8046 Garching, Germany

H. Schneuwly
Los Alamos National Laboratory, Los Alamos, New Mexico 87545
and University of Fribourg, CH-1700 Fribourg, Switzerland
(Received 14 January 1983)

Muonic x-ray spectra have been measured for N_2, SF_6, and Ar at pressures up to 20 atm at room temperature and in the liquid or solid state, and for O_2 at 20 atm and CO, NO, and a N_2+O_2 mixture at 10 atm. Relative intensities of the higher members of the muonic Lyman series of N decrease monotonically with decreasing pressure (density). A similar effect is observed for F in SF_6, where some effect was also noted for the S x rays. A gas-pressure dependence in Ar was not observed in the pressure range covered. The density effect can be modeled approximately by a muonic-atom cascade code in which the K-electron refilling width is related to the gas density, which determines the frequency of collision of the atom with neighboring atoms or molecules. The difference in behavior between N_2 or SF_6 and Ar at comparable pressures provides evidence for the "Coulomb explosion" that is expected to occur when a negative muon is captured by a polyatomic molecule.

I. INTRODUCTION

The muonic x-ray spectrum generated when negative muons are stopped in a given target material is a function of both the chemical constitution (elemental composition and molecular structure) and the physical state (density, particle size in mixtures, etc.) of that material. This dependence arises at two different stages in the stopping process. The first stage, the Coulomb capture of the muon by an atom or molecule, depends on the capture cross section and muon flux density, the dependence of both these parameters on muon energy being affected by the electronic structure of the stopping material. To the extent that the electronic structure is affected, the initial population of bound muon states may vary with physical state; variations in density alone, on the other hand, as with gas targets, are expected to have little effect. The second stage in the stopping process, the muonic de-excitation cascade in the capturing atom, should be sensitive to density. The cascade proceeds in large part with Auger electron emission, depleting the atom's electrons. The rate and levels at which these electrons are replaced by collisions with neighboring atoms or molecules affect the competition between Auger and radiative channels in the cascade, and thus they can influence the muonic x-ray intensity distribution resulting from a given capture population. This effect should be observable in gas targets as a variation of the muonic x-ray intensity pattern with pressure. Measurements of this variation would allow one to study the de-excitation cascade by adjusting the electron refilling rate without affecting the nature of the Coulomb capture process. Although the electron depletion effect has been recognized for some time,[1-3] it has only recently been addressed experimentally.[4-8]

We report here some results we have obtained in an exploratory study of the pressure (density) effect in N_2, SF_6, and Ar at pressures up to 20 atm at room temperature and in the liquid or solid state, together with some relevant data on the gases CO, O_2, and a N_2+O_2 mixture. We compare the experimental muonic x-ray intensity patterns with the predic-

tions of a cascade code[9] incorporating various adjustable inputs for the muonic n and l distributions at some stage after Coulomb capture and for electron shell populations during the cascade.

II. EXPERIMENTAL PROCEDURES

The experiments were carried out at the stopped muon channel of the Clinton P. Anderson Meson Physics Facility (LAMPF), using 82- or 90-MeV/c negative muons with a momentum bite $\Delta p/p$ about $\pm 5\%$ and beam duty factor 6 to 7%. The experimental arrangement for the gas targets is sketched in Fig. 1. Two kinds of gas cell were employed: for the N_2, O_2, SF_6, and Ar, a steel cylinder 58 cm long and 15 cm in diameter with walls 3 mm thick in a 9-cm wide band around its middle; for the N_2+O_2 mixture, the NO, and CO, an aluminum cylinder 32 cm long and 13.3 cm in diameter with walls 7 mm thick. Gas pressures were measured with a precision Bourdon-type gauge. The liquid N_2, liquid Ar, and solid SF_6 targets were contained in thin-walled polyethylene bags in a Styrofoam container; the N_2 gas target at 0.77 atm (local pressure) consisted of pure N_2 gas in a thin-walled polyvinyl chloride bag, large enough so that muon stops occurring in the bag wall material were registered only very inefficiently in the x-ray detector.

The detector used for the high-Z targets Ar and SF_6 was an ORTEC coaxial Ge(Li) unit with 10% nominal efficiency; for the low-Z targets, the detector used was an intrinsic Ge cylinder 3.6 cm in diameter and 1.2 cm thick, manufactured by Princeton Gamma-Tech. In all cases the detectors were shielded by copper or lead "blinders" at either side so that they could not see radiation emitted from muon stops in the ends of the gas cells. The muon beam collimator nearest the target cell was set typically at 2.5 to 3.5 cm aperture. The beam energy degraders were adjusted in each case to produce the peak in the stopping distribution near the midpoint of the cell. In the processing of the muonic x-ray data, account was taken of the spatial distribution of the muon stops in the target.

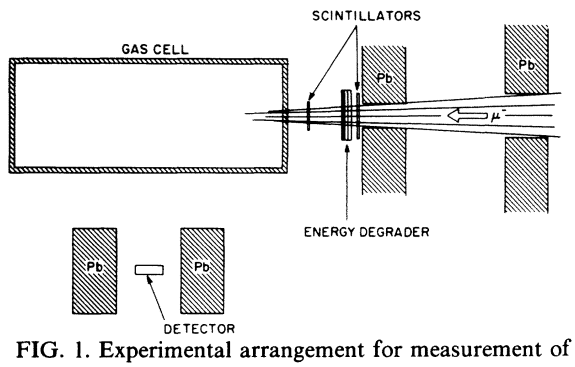

FIG. 1. Experimental arrangement for measurement of muonic x-ray spectra of gas targets.

To keep the gas cell and target systems as simple and as light as possible, we omitted the veto scintillator usually employed to signal that an entering muon failed to stop in the target material of interest. Instead, an analyzable event was defined by coincidence of a Ge detector pulse with pulses from the two scintillators ahead of the target. The resulting spectra in most cases contained a significant component from stops in the walls of the gas cell, but in only a few cases was there significant interference with the x rays of interest. Details of the detector plus pulse-height-analyzer system are given in Ref. 10.

Analysis of the recorded muonic x-ray spectra was carried out with an adaptation of the peak-fitting program SAMPO.[11] Determination of the relative overall detector counting efficiencies of the various x rays generated in each gas target was performed with a local distributed-source code.[12] The distribution of muon stops in the gas varied with gas composition and density, and had to be approximated for introduction into the geometric parameters of the code. At the temperatures and pressures employed in these experiments the SF_6 density departed significantly from that of an ideal gas and was calculated from published equation-of-state data.[13]

III. RESULTS AND DISCUSSION

A. Ar and SF_6

Our measurements on Ar and SF_6 were intended to compare the muonic x-ray spectra of two elements of comparable Z in strongly differing chemical environments. The Ar is monatomic and chemically unbound; its muonic atom after Coulomb capture has a kinetic energy little over thermal. The S atom, however, is chemically bound before Coulomb capture of the muon. After capture, the chemical bonds are broken as a result of Auger-electron emission accompanying the muonic atom de-excitation cascade. This electron loss leads to a "Coulomb explosion" in which the positive muonic S ion is repelled by its former bonding partners, yielding several electron volts of kinetic energy. Muon capture on one of the F atoms leads to a similar result.

Muonic x-ray spectra of Ar were measured for three different target states: the liquid near its boiling point at local pressure, and the gases at 20 atm and at 5 atm, both at room temperature. The experimental x-ray intensities are summarized in Table I, together with the corresponding intensities calculated from the muon cascade model.[9] The cascade code parameters were first set to fit the intensity ra-

TABLE I. Muonic x-ray intensities of argon.

Density (g/cm^3) =	Liquid, −186 °C 1.40			Gas, 20 atm, 22 °C 33×10^{-3}			Gas, 5.0 atm, 22 °C 8.3×10^{-3}
Intensity ratio ($\times10^3$)	Experiment[a]	Cascade model	χ_i^2	Experiment[a]	Cascade model	χ_i^2	Experiment[a]
$K\beta/K\alpha$	73.7± 1.5	74.41	0.22	41.4± 1.6	42.55	0.82	41.9± 2.5
$K\gamma/K\alpha$	26.4± 1.1	26.61	0.04	10.7± 1.4	9.51	0.72	10.6± 1.6
$K\delta/K\alpha$	22.6± 1.0	23.20	0.36	9.0± 2.0	4.96	4.08	9.6± 2.0
$K\epsilon/K\alpha$	15.0± 1.0	16.78	3.17		5.57		
$K\zeta/K\alpha$	11.1± 1.0	9.38	2.96	9.8± 2.0	8.11	0.71	9.0± 2.0
$K\eta/K\alpha$	4.6± 1.0	4.21	0.15	6.1± 2.0	6.85	0.14	6.3± 2.0
$K\theta/K\alpha$	4.2			2.5± 1.5	1.68	0.30	
$L\alpha/K\alpha$	722 ±30	793.0	5.60	921 ±60	876.4	0.55	902 ±60
$L\beta/K\alpha$	101 ± 5	124.8		83			78
$L\gamma/K\alpha$	32.7± 2.0	55.7		32.1± 3.2			28.0± 3.0
$L\delta/K\alpha$	19.6± 2.0	25.4		17.5± 2.0			18.7± 2.0
$L\epsilon/K\alpha$	7.0± 0.7	9.72					
Muonic atom cascade parameters							
n_μ (initial)		14			14		
$\alpha(l$ distribution)		+0.15			+0.15		
K electrons (initial)		2			2		
K refill width (eV)		0.30			0.0003		
$L+M$ electrons (initial)		16			16		
$L+M$ population		No depletion			No refilling		

[a]Experimental errors shown are one standard deviation $\chi_i=$(cascade-experiment)$/\sigma$.

tios for the liquid target: the initial electron population was set with the K, L, and M shells filled (i.e., the neutral muonic atom) and the L and M shells were kept filled throughout the cascade, the K-electron refilling width ($=\hbar/t$) was set near the isolated-atom value,[14] ~0.5 eV. The muon cascade was started from $n_\mu=14$ with population of the l substates distributed according to a modified statistical distribution function $P(l)\propto(2l+1)\exp(\alpha l)$ with α adjustable. Whether or not the L and M electron shells were kept filled or allowed to deplete as a result of Auger processes had only a relatively small effect on the intensity pattern.

Setting the K electron width equal to 0.3 eV and $\alpha=+0.15$ gave the best fit to the muonic Lyman intensity ratios, with the χ_i^2 values shown. The poor fits for $K\epsilon/K\alpha$ and $K\zeta/K\alpha$ probably reflect unaccounted-for background under these weak peaks. Thus we see that, in general, our simple model with two adjustable parameters gives a satisfactory fit to the Lyman intensity data. The corresponding fit for the Balmer intensities is not as good; the model consistently overestimates these transitions even if we take into account that a given set of transitions, say from $n=4$ to $n=2$, may represent an energy spread of several keV.

If we assume the angular distribution of captured muons at $n=14$ is approximately the same for liquid Ar as for gaseous Ar, then the same $\alpha=+0.15$ may be used for the cascade fit to the latter. We see from the χ_i^2 values that a satisfactory fit to the observed 20-atm Lyman intensities (except for $K\epsilon/K\alpha$) can be obtained. In this case, the cascade calculation was started with neutral Ar and allowed to proceed without any refilling of the L and M shells; the K width was set at 3×10^{-4} eV. A zero K width would have fitted almost as well. We note also that the experimental intensity pattern for Ar at 5 atm is not significantly different from that at 20 atm.

We may use some simple approximations to estimate whether this K width is reasonable. By tracking the muon cascade from Coulomb capture down to $n=7$ and estimating the random-walk effect of the recoil from the Auger electrons on the kinetic energy of the muonic Ar atom, we find that its velocity should be of the order of 8×10^4 cm/s. Assuming a charge-transfer radius of 3.85 Å (the diameter of the neutral Ar atom), we obtain for the 20-atm target an average time to first collision of about 5×10^{-12} s, corresponding to a width of about 1.3×10^{-4} eV. Since the muonic de-excitation cas-

cade to the lower levels occurs on a time scale of the order of 10^{-14} s as long as a few electrons remain, the muonic Ar atoms even at 20 atm should behave essentially the same as at very low pressures. A noticeable change in the Ar muonic x-ray spectrum should require substantially higher pressures, but should then set in rapidly owing to multiple-collision effects; once the first electron transfer has occurred, the muonic atom acquires several eV of kinetic energy and the time between subsequent collisions is reduced by an order of magnitude.

The comparable set of measurements for muons stopped in the molecular species SF_6 is summarized in Table II, where we tabulate muonic x-ray intensities for the F and the S under three target conditions: solid SF_6 near the sublimation point (about $-64\,^{\circ}C$), and gaseous SF_6 at $22\,^{\circ}C$ and absolute pressures of 20.59 atm and 4.94 atm. Intensity fits with a cascade model are also shown. As with the analysis of the Ar results, we use the data for the condensed phase as the first point of reference in the fitting procedure. We start the de-excitation cascade at $n_\mu = 14$, all electron shells are assumed to be initially filled and the L and M shells remain filled, while K-electron refilling widths are set at 0.16 eV and 0.5 eV for F and S, respectively.[14] We adjust α in the muon angular momentum distribution function $P(l) \propto (2l+1)\exp(\alpha l)$ to obtain best fits. If once again we assume that the muon angular momentum distribution at $n_\mu = 14$ is the same for the gas systems as for the solid, then we can use the optimized α from the solid and seek the gaseous sample K widths which give the best fits to the experimental data. The best cascade parameters obtained by this procedure are listed at the bottom of Table II.

An examination of the data and the resulting fits shows several features of interest:

(1) for fluorine, the muonic Lyman and Balmer spectra of the solid target and the Lyman spectra of the gas targets (the Balmer spectra were too strongly absorbed in the pressure-vessel walls) are fitted well by the simple cascade model; the apparent K-electron vacancy widths for the gas targets decrease with decreasing gas density, although a factor of 6 change in gas density results in only a factor of 3 change in width;

(2) for sulfur, the muonic x-ray spectra of the three targets can be fitted with simple cascade models, but the experimental intensity patterns for the two gas pressures are so similar that they cannot reasonably be assigned different cascade parameters on the basis of our data; the best fit α for the gas targets does appear to be significantly higher, however, than that for the solid target;

(3) the best fit α for the muonic fluorine is markedly lower than that for the muonic sulfur, and the latter, in turn, is significantly lower than that for muonic argon, suggesting that the average muon angular momentum at $n_\mu = 14$ increases in the sequence F-S-Ar.

A puzzling feature of these data is the difference in the Lyman intensity pattern trends for the F and the S from the gaseous SF_6 targets. The higher Lyman members of the F clearly decrease with decreasing target pressure, whereas those of the S appear to be the same at the two pressures. Although the experimental errors in the S data are relatively large, the effect (and the difference relative to F) is real and must be taken into account in future measurements and in the evaluation of theoretical models. A possible source of the difference may lie in the structure of the SF_6 molecule. The sulfur atom is enclosed in a "cage" of fluorine atoms, and after muon capture it may acquire from them some electrons to replace those lost in the early stages of the de-excitation cascade, before the elements of the molecule fly apart. A fluorine atom, on the other hand, may be more likely to escape its neighbors immediately following muon capture, and thus its de-excitation cascade could be affected more by the density of other molecules available as collision partners.

Analysis of the muonic x-ray spectra of the SF_6 targets also permitted the extraction of data bearing on the question of whether the F/S Coulomb capture ratio is a function of the physical state of the SF_6. Summation of the absolute intensities of the muonic K x rays of the fluorine and the sulfur gave the intensity ratios listed at the bottom of Table II. Disregarding possible very small differences in the fraction of muon captures leading to K x rays as a function of physical state (results of the cascade code indicate that the K x rays per muon capture range from 0.966 to 0.973 for sulfur and 0.951 to 0.961 for fluorine), we see that the F/S capture ratio is constant within experimental error. The weighted average F/S capture ratio, taking into account the calculated x ray per muon corrections and systematic errors, is 6.43 ± 0.25. The only previous measurement of the F/S capture ratio,[15] 7.4 ± 1.0, is consistent with ours, both results indicating a factor-of-2 deviation from the "Z Law" in favor of the fluorine but agreeing well with the value predicted by the formulation of Schneuwly *et al.*,[16] with the use of a S—F bond ionicity from Pauling[17]: a F/S capture ratio of 6.17.

B. C, N, and O

Our measurements on the three light elements C, N, and O were made up of two sets. The first set,

TABLE II. Muonic x-ray intensities of F and S in SF_6.

Density (g/cm^3) =	SF_6 solid, −64 °C 1.88			SF_6 gas, 20.59 atm, 22 °C 194×10^{-3}			SF_6 gas, 4.94 atm, 22 °C 31.6×10^{-3}		
Intensity ratio ($\times10^3$)	Experiment[a]	Cascade model	χ_i^2	Experiment[a]	Cascade model	χ_i^2	Experiment[a]	Cascade model	χ_i^2
				Fluorine					
$K\beta/K\alpha$	211.3± 6.3	213.0	0.18	163.5±5.6	162.7	0.02	125.9±5.0	129.2	0.44
$K\gamma/K\alpha$	183.2± 6.4	179.4	0.35	134.4±5.2	136.1	0.11	94.9±4.1	94.9	0.00
$K\delta/K\alpha$	99.3± 4.0	98.3	0.06	96.2±3.9	95.2	0.07	85.8±3.9	80.4	1.92
$K\epsilon/K\alpha$	32.9± 3.3	33.8	0.07	48.4±2.2	46.5	0.75	56.3±2.9	52.8	1.46
$K\zeta/K\alpha$	9.5± 2.4	9.8	0.02	15.6±1.4	17.7	2.25	18.6±3.9	25.6	3.22
$K\eta/K\alpha$				3.6±1.4	5.9	2.70	13.4±4.4	11.0	0.30
$L\alpha/K\alpha$	623 ±187	748	0.45						
$L\beta/K\alpha$	161 ± 32	153	0.06						
$L\gamma/K\alpha$	56 ± 11	43	1.40						
$L\delta/K\alpha$	23 ± 11	11	1.19						
Muonic atom cascade parameters									
n_μ(initial)		14			14			14	
$\alpha(l$ distribution)		−0.015			−0.015			−0.015	
K electrons (initial)		2			2			2	
K refill width (eV)		0.16			0.025			0.009	
$L+M$ electrons (initial)		8			8			8	
$L+M$ population		No depletion			No refilling			No refilling	
				Sulfur					
$K\beta/K\alpha$	109.3± 4.4	101.9	2.83	75.0± 5.0	81.4	1.64	81.4± 6.5	81.4	0.00
$K\gamma/K\alpha$	53.0± 3.2	53.3	0.01	33.7± 2.5	32.8	0.14	33.8± 5.7	32.8	0.03
$K\delta/K\alpha$	48.4± 3.4	51.9	1.06	33.5± 2.6	31.7	0.48	39.2± 6.1	31.7	1.51
$K\epsilon/K\alpha$	35 ± 6	37.6	0.19	30.9± 2.5	28.5	0.92	17.5± 5.6	28.5	3.86
$K\zeta/K\alpha$	17.4± 2.8	17.1	0.01	12.1± 2.5	16.1	2.56			
$K\eta/K\alpha$	12.2± 2.7	7.7	2.78	6.4± 2.0	6.9	0.06			
$L\alpha/K\alpha$	665 ±30	722	3.61	722 ±80	776	0.46	733 ±130	776	0.11
$L\beta/K\alpha$									
$L\gamma/K\alpha$				72 ± 8	63.6	1.10			
Muonic atom cascade parameters									
n_μ(initial)		14			14			14	
$\alpha(l$ distribution)		+ 0.07			+ 0.10			+ 0.10	

TABLE II. (*Continued.*)

Density (g/cm^3) =	SF_6 solid, −64 °C 1.88			SF_6 gas, 20.59 atm, 22 °C 194×10^{-3}			SF_6 gas, 4.94 atm, 22 °C 31.6×10^{-3}		
Intensity ratio ($\times10^3$)	Experiment[a]	Cascade model	χ_i^2	Experiment[a]	Cascade model	χ_i^2	Experiment[a]	Cascade model	χ_i^2
K electrons (initial		2			2			2	
K refill width (eV)		0.50			0.09			0.09	
$L+M$ electrons (initial)		16			16			16	
$L+M$ population		No depletion			No refilling			No refilling	
$\frac{\sum FK \text{ x rays}}{\sum SK \text{ x rays}}$		6.37±0.30			6.54±0.45			5.96±0.50	

[a]Experimental errors shown are one standard deviation. $\chi_i=$(cascade−experimental)/σ.

involving targets of gaseous N_2 at room temperature and pressures from 0.77 to 20 atm, was intended to compare muonic x-ray spectra up to densities at which the time between Nμ ion-N_2 collisions is comparable to the time scale of the Nμ de-excitation cascade. It included also a measurement of the spectrum of liquid N_2 as a condensed-phase reference point for the same target molecule. The second set was intended primarily to compare the N/O muon capture ratio for NO gas with that for N_2+O_2 under essentially identical conditions to elicit in a simple way the effect of bonding unlike atoms; a similar measurement was made on CO gas to provide additional information on this effect. The relative capture data from these experiments have been discussed in a previous report.[18] Also included in this second group is the muonic Lyman spectrum for O_2 gas at 20 atm.

The muonic x-ray spectra of nitrogen are summarized in Table III, which lists the Lyman intensities in terms of ratios to the $2p\rightarrow1s$ transition intensity in each case. The muonic Balmer series x rays were too strongly absorbed by the container walls to permit useful measurement except for the 0.77-atm target, where the only wall between target and detector system was the thin polyvinyl chloride bag.

The most conspicuous feature of these data is the monotonic decrease in the relative intensities of the upper members of the Lyman series with decrease in gas density, in qualitative agreement with expectations. As the frequency of collisions of the muonic atom with electron-replacing molecules decreases, the Auger de-excitation channels are suppressed in favor of the radiation channels, where the transitions have larger average Δn. These radiative processes favor population of the muonic $l=n-1$ states, whence further radiative excitation leads to $2p\rightarrow1s$ transitions.

We have compared our experimental data with the output of the muonic atom cascade code incorporating the following assumptions: cascades started at $n_\mu=14$ with angular momentum states populated according to $P(l)\propto(2l+1)\exp(\alpha l)$, muonic atoms initially neutral (e.g., Nμ $1s^22s^22p^2$), the $1s$ electrons replaced at a rate expressed by a K width, the other electrons either maintained at their initial population (for liquid N_2) or not replaced (for the gases). In addition, the electron K width for the atoms in gas targets is constrained to be proportional to gas pressure—this means, in practice, that the model chosen for muonic nitrogen, say, must fit the data for all three pressures with a single adjustment to the K width scale.

A representative fit for muonic nitrogen is shown in Fig. 2, where we plot the Lyman intensity ratios as a function of electron K width for the three gas

TABLE III. Muonic x-ray intensities of nitrogen.[a]

	N_2 liquid	N_2 gas, 20 atm	N_2 gas, 5.0 atm	N_2 gas, 0.77 atm	N_2, 5.0 atm + O_2, 5.0 atm	NO, 10.0 atm
Density (g/cm^3) =	0.81	23.1×10^{-3}	5.8×10^{-3}	0.90×10^{-3}	12.4×10^{-3}	12.4×10^{-3}
Intensity ratio ($\times10^3$)						
$K\beta/K\alpha$	202±5	101.7±3.0	64.2±3.6	47.9± 1.3	86.8±3.3	95.0±3.0
$K\gamma/K\alpha$	109±5	51.8±3.1	33.2±5.4	27.1± 6.0	46.9±5.0	48.9±5.0
$K\delta/K\alpha$	38±3	27.2±2.8	19.3±5.8	19.1± 6.0	30.8±5.5	27.5±5.5
$K\epsilon/K\alpha$		16.5±5.0	16.2±6.4			
$L\alpha/K\alpha$				781 ±78		
$L\beta/K\alpha$				52.1± 3.1		
$L\gamma/K\alpha$				22.1± 1.5		
$L\delta/K\alpha$				18.5± 1.3		
$L\epsilon/K\alpha$				15.0± 1.3		
$L>\epsilon/K\alpha$				7.3± 1.3		

[a]Liquid N_2 target at -196 °C and, gas targets at 22 °C.

pressures and for the liquid state. Also included are data points for muonic nitrogen in the N_2+O_2 mixture and in the NO gas. We see, first of all, that the fit of the model to the experimental data for the gases is generally satisfactory, although the experimental $K\gamma/K\alpha$ and $K\delta/K\alpha$ points deviate somewhat at the lowest pressure. The only adjustable parameters in this fit were the angular momentum distribution constant α, which we set at $+0.14$, and the fit to the K width scale. Within the rather large experimental errors of the intensity ratios beyond $K\beta/K\alpha$, the fit shown is not unique; decreasing the value of the parameter α increases the relative population of low-l initial muon states and thus the relative intensity of the higher $np\rightarrow1s$ transitions, and decreasing the initial population of the $2s$ and $2p$ electron orbitals decreases the intensity of the higher $np\rightarrow1s$ muonic transitions. The shapes of the $Ki/K\alpha$ curves such as those shown in Fig. 2 are relatively insensitive to small changes in the angular momentum distribution and electron L shell population parameters; adjustment of these parameters simply moves the set of curves to the left or right on the plot (i.e., changes the K width scale by a constant). From trial parameter adjustments of this kind we find that our data are fitted by $\alpha=+0.14\pm0.04$ and by a K-electron width scale in which 20 atm corresponds to a width of $\sim3.6\times10^{-3}$ eV (to within a factor of 2). This width may be estimated independently from gas-kinetic considerations. If the $N\mu$ ion is assumed to have an average kinetic energy of 6.6 eV (from the repulsion of two singly charged ions starting at the N_2 molecule bond distance) and its effective radius for charge exchange with a N_2 molecule is taken to be 3.9Å, then the average time between collisions at 20 atm and room temperature is 4.5×10^{-13} s, corresponding to a width of 1.5×10^{-3} eV. In view of the gross approximations involved in modeling the muonic atom de-excitation cascade and concurrent electron-refilling processes by a single K electron width, on the one hand, and in estimating the product of $N\mu$ ion velocity and charge-exchange cross section, on the other, it is of interest to note the consistency of these estimates.

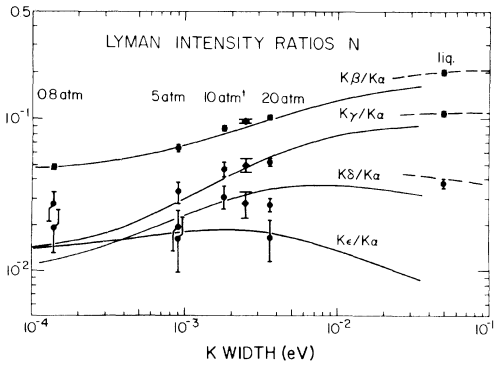

FIG. 2. Comparison of experimental muonic Lyman x-ray intensity ratios for nitrogen with predictions of a cascade model. Circular points represent data from muon capture in N_2, diamonds represent capture in NO at 10 atm; target designated "10 atm†" was 5 atm N_2+5 atm O_2. Curves represent cascade model ratios as a function of K electron refilling width, fitted to data as described in the text.

We remark on three other aspects of the data plotted in Fig. 2. The first concerns the muonic Lyman intensity patterns for the nitrogen in N_2+O_2 and in NO. The pattern for the N_2 in the mixture should be about the same as that for the pure N_2 gas except for a small difference in the K width scale

TABLE IV. Muonic x-ray intensities of oxygen[a] and carbon.

	O_2 gas, 20 atm	N_2, 5.0 atm $+O_2$, 5.0 atm	NO, 10.0 atm	CO, 10.0 atm
Density (g/cm^3) =	26.4×10^{-3}	12.4×10^{-3}	12.4×10^{-3}	11.6×10^{-3}
Intensity ratio ($\times10^{3}$)				
		Oxygen		
$K\beta/K\alpha$	83.2±10.2	69.7±2.9	70.8±3.0	81.2± 2.8
$K\gamma/K\alpha$	40.7±2.2	35.1±3.5	41.3±2.4	31.0± 2.4
$K\delta/K\alpha$	26.8±2.0	29.3±2.7	31.3±3.0	25.1± 3.2
$K\epsilon/K\alpha$	26.1±2.7	15.8±3.1		16.6± 3.2
		Carbon		
$K\beta/K\alpha$				
$K\gamma/K\alpha$				

N_2+O_2: $\frac{\sum NK \text{ x rays}}{\sum OK \text{ x rays}} = 0.834\pm0.031$

NO: $\frac{\sum NK \text{ x rays}}{\sum OK \text{ x rays}} = 0.959\pm0.030$ $\qquad \frac{(N \text{ x rays/O x rays})_{mixture}}{(N \text{ x rays/O x rays})_{NO}} = 0.870\pm0.032$

CO: $\frac{\sum CK \text{ x rays}}{\sum OK \text{ x rays}} = 0.766\pm0.030$

[a]All targets at 22 °C.

due to a difference in the N_2 and O_2 charge-exchange cross sections. We see that this is the case. Although we have plotted the data points as if the target gas were pure N_2, the fit could have been improved by locating them at a K width 1.3-fold higher, implying a larger charge-exchange cross section for the O_2. The muonic nitrogen points for the NO gas target have also been included in the plot, though the muon capture process is not expected to be the same as for N_2. It is evident that the difference is small.

A second aspect has to do with the disturbing failure to obtain good fits for the $K\gamma/K\alpha$ and $K\delta/K\alpha$ intensity ratios at the lowest pressure. Both experimental values are well above those predicted by the model in this K electron width range, and no reasonable adjustments in the model parameters appear to alleviate the problem; the muonic Balmer intensity ratios are not sufficiently sensitive to parameter changes to provide a useful guide. At this point the most useful approach to the problem would be more precise experimental data in the low pressure region.

Finally, we see that the experimental intensity ratios for the liquid N_2 target lie well above the model predictions that best fit the gas target data, even with the cascade conditions modified so that the L electron shell is maintained full. If our simple model is to fit the liquid N_2 as well, we may have to allow for a change in a quantity that we have thus far held constant, namely, the initial muonic angular momentum distribution. By lowering the parameter α to $+0.095$, we indeed obtain an excellent fit for the Lyman intensity ratios of the liquid N_2 target, given a K electron width near 0.05 eV.

Thus, our simple model suggests that muons are captured at lower angular momentum in liquid-phase N_2 than in gas-phase N_2. This conclusion is consistent, in turn, with the expected difference in the outer tail of the molecular electron distribution: in a condensed phase, this tail is confined by neighboring molecules. Accordingly, average angular momenta of muons captured under these conditions should be smaller.

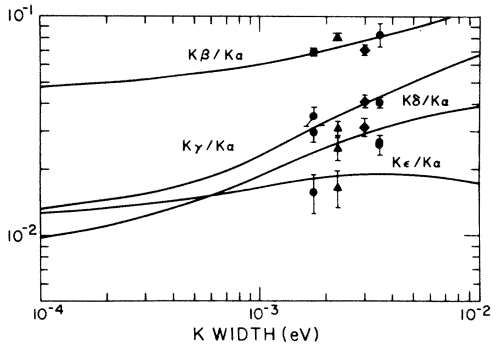

FIG. 3. Comparison of experimental muonic Lyman x-ray intensity ratios for oxygen with predictions of a cascade model. Circular points: muon capture in O_2 (left, 5 atm N_2+5 atm O_2; right, 20 atm O_2). Diamonds: capture in 10 atm NO. Triangles: capture in 10 atm CO. Curves represent cascade model ratios as a function of K electron refilling width, fitted to data as described in the text.

The muonic Lyman intensity ratios for oxygen (in O_2 at 20 atm, N_2+O_2 at 10 atm total, NO at 10 atm, and CO at 10 atm) and for carbon (in CO at 10 atm) are listed in Table IV. The data for oxygen are plotted in Fig. 3, together with the corresponding ratios calculated from a cascade model fitted approximately to the data. Although the experimental data at only two pressures are insufficient to permit the evaluation of a specific set of cascade parameters, we find that a cascade starting at $n_\mu = 14$ and $\alpha = +0.14$ and with a filled initial electron population $1s^2 2s^2 2p^3$ with no subsequent refilling of the L shell electrons gives a reasonable fit. The K-electron width scale associated with this fit is such that muonic x-ray data for the 20-atm target correspond to a K-electron width of $\sim 3.5 \times 10^{-3}$ eV, a value essentially indistinguishable from that for the N_2 target at the same pressure. We include in the plot the data points for the NO and CO targets, although the model parameters would not be expected to be the same as for oxygen in O_2; also, our choice of position on the K-width scale was chosen for best fit. We see, indeed, that the experimental Lyman intensity patterns for oxygen in the N_2+O_2 mixture and in NO are very nearly the same. The pattern for oxygen in CO, on the other hand, appears to be significantly different and would be better fitted by a model with higher α, that is, by higher average angular momentum of the muons in the capture state(s).

IV. SUMMARY

Our principal results and conclusions from this investigation may be summarized as follows. In low-Z gas targets we find that the relative intensities of the higher members of the muonic Lyman series x rays decrease monotonically with decreasing gas density. This correlation can be modeled approximately by the use of a muonic-atom cascade in which the K-electron refilling width is related to the mean time-to-collision. Collision times for muonic atoms from polyatomic gases can be expected to be much shorter than for monatomic gases if a "Coulomb explosion" occurs when the negative muon is captured into a polyatomic molecule; our data provide evidence supporting this mechanism.

Future work can improve these studies in at least two ways. First, the cascade model could be made more realistic by distributing the initial muon population in n and l rather than l only, and/or by selecting a more complex l distribution. Given the simplicity of the model we have employed in this study, however, we doubt that further complication in parameter adjustments is justified. More importantly, the electron-refilling collisions might be introduced at various steps in the cascade, perhaps in a Monte Carlo fashion, instead of by a simple adjustment of the K-electron width as we have done. Before such calculational improvements could be justified, additional data should be available. In particular, it would be useful to have (1) lower errors for the higher Lyman transitions and additional lines for the Balmer spectra; (2) for N_2, measurements at pressures greater than 20 atm and in the vicinity of 1 atm; and (3) oxygen measurements over a wider range of presssures for O_2 and for CO and NO.

ACKNOWLEDGMENTS

We express our gratitude to Dr. D. C. Hagerman and the accelerator operating team at the Clinton P. Anderson Meson Physics Facility (LAMPF) at Los Alamos for their support and cooperation, and to Dr. J. E. Sattizahn and the staff of the Nuclear Chemistry group for their essential support throughout the course of this work. We are indebted to Mr. Fred Loeser for his ingenuity and craftsmanship in setting up and introducing us to the operation of the compressed gas management system and gas targets. We thank Professor H. Daniel for valuable consultation and advice in the analysis of our work. Three of (R. A. N., F. J. H., and H. S.) wish to express our thanks to the staff of the facility, in particular Dr. L. Rosen, for assistance they received during their stay at Los Alamos. The work at LAMPF was performed under the auspices of the U. S. Department of Energy.

[1]E. Fermi and E. Teller, Phys. Rev. 72, 399 (1947).

[2]H. Daniel, Naturwissenschaften 55, 314 (1968).

[3]H. -J. Pfeiffer, K. Springer, and H. Daniel, Nucl. Phys. A254, 433 (1975).

[4]A. L. Carter *et al.* (unpublished), as communicated by C. K. Hargrove (private communication).

[5]R. Bergmann, H. Daniel, P. Erhart, F. J. Hartmann, H. -J. Pfeiffer, J. J. Reidy, T. von Egidy, and W. Wilhelm, Abstracts of Contributed Papers, 8th International Conference on High Energy Physics and Nuclear Structure, Vancouver, Canada, August, 1979 (unpublished).

[6]J. D. Knight, C. J. Orth, M. E. Schillaci, R. A. Naumann, F. J. Hartmann, J. J. Reidy, and H. Schneuwly, Ref. 5 (unpublished).

[7]P. Ehrhart, Los Alamos Report Number LA-8835-C, 1981 (unpublished).

[8]J. D. Knight, Los Alamos Report LA-8835-C, 1981 (unpublished).

[9]V. R. Akylas and P. Vogel, Comput. Phys. Commun.

15, 291 (1978).
[10]C. J. Orth, M. E. Schillaci, J. D. Knight, L. F. Mausner, R. A. Naumann, G. Schmidt, and H. Daniel, Phys. Rev. A 25, 876 (1982).
[11]J. T. Routti and S. G. Prussin, Nucl. Instrum. Methods 72, 125 (1969); adapted for Los Alamos use by B. R. Erdal.
[12]R. L. Hutson, private communication.
[13]H. P. Clegg, J. S. Rowlinson, and J. R. Sutton, Trans. Faraday Soc. 51, 1327 (1955).
[14]O. Keski-Rahkonen and M. O. Krause, At. Data Nucl. Data Tables 14, 139 (1974).
[15]H. Daniel, H. -J. Pfeiffer, and K. Springer, Phys. Lett. 44A, 447 (1973).
[16]H. Schneuwly, V. I. Pokrovsky, and L. I. Ponomarev, Nucl. Phys. A312, 419 (1978).
[17]L. C. Pauling, *The Nature of the Chemical Bond and the Structure of Molecules and Crystals,* 3rd ed. (Cornell University Press, Ithaca, New York, 1960).
[18]J. D. Knight, C. J. Orth, M. E. Schillaci, R. A. Naumann, F. J. Hartmann, J. J.Reidy, and H. Schneuwly, Phys. Lett. 79A, 377 (1980).